12th International Conference on Fracture Mechanics of Concrete and Concrete Structures
FraMCoS-12
B.L.A. Pichler, Ch. Hellmich, P. Preinstorfer (Eds)

https://doi.org/10.21012/FC12.1343
MS07-2:4

SALTWATER FLOODING-INDUCED CORROSION AND LATERAL STRENGTH OF REINFORCED CONCRETE STRUCTURES

ERIK W. BENSON*, RAVI RANADE*, PINAR OKUMUS*, NEGAR ELHAMI-KHORASANI*, OCEANA FRANCIS† AND REBEKAH PACI-GREEN‡

* State University of New York, University at Buffalo, Department of Civil, Structural and Environmental Engineering
212 Ketter Hall University at Buffalo, Buffalo, NY 14260, USA

† University of Hawaii, Manoa, Department of Civil, Environmental and Construction Engineering and Sea Grant College Program
2540 Dole Street, Holmes 383, Honolulu, Hawaii 96822, USA

‡ Western Washington University, Department of Environmental Studies
516 High Street, MS 9085, Bellingham, WA 98225

Key words: Coastal, chloride, moment frame, seismic, deterioration, pushover

Abstract: Many coastal communities are located in areas of high seismic activity. Saltwater flooding can exacerbate the corrosion of lateral force-resisting systems of structures in these communities, impacting their seismic resilience. Evaluating the compounding risk from flood and seismic hazards in these communities is a necessary step toward ensuring the safety of coastal populations and infrastructure. This paper studies the loss of rebar in coastal reinforced concrete buildings over time due to both atmospheric and saltwater flooding-related corrosion and evaluates their effects on the performance of the lateral load resistance of these buildings. A previously developed corrosion model was modified to incorporate the impacts of annual coastal flooding on the corrosion rate. Finite element models of a reinforced concrete moment frame were created with rebar cross-sectional areas corresponding to various levels of corrosion. Pushover analyses were performed to determine the lateral strength and ultimate displacement capacity under different scenarios: atmospheric corrosion only, lower- and upper-bound corrosion rate changes due to flooding, corrosion of exterior columns or all columns due to flooding, and varying exposure durations (60 years or 80 years). The results show that although atmospheric corrosion does not lead to considerable change in lateral response, annual coastal flooding may result in up to 26% loss in lateral strength and up to 83% loss in displacement capacity. When the post-cracking corrosion rate is assumed to be four times higher than the pre-crack corrosion rate, the strength loss for buildings where all first-floor columns flooded becomes significant (>20%) over an 80-year period. In contrast, the displacement capacity loss is more sensitive to corrosion; even when the corrosion rate is assumed to simply double after cracking, with only the exterior columns exposed to seawater, displacement capacity decreases significantly (>10%) after 60 years.

1 INTRODUCTION

This study aims to understand how the compounding hazards of coastal flooding, chloride-induced deterioration, and seismicity impact the performance of coastal reinforced concrete (RC) structures. Unlike atmospheric exposure, which gradually increases the chloride concentration within RC structures,

coastal flooding can cause a sudden exposure to chlorides due to seawater having salt concentrations over 30 g/m^3 [1], while typical atmospheric concentrations of sea salt range from 0.3 to 3 $\mu g/m^3$ [2]. Thus, coastal structures experience chloride deposition due to both airborne chlorides in the coastal atmosphere and salts dissolved in seawater.

Many regions in the United States deemed to be at risk of coastal flooding are also located in areas of high seismicity [3, 4]. The American Concrete Institute (ACI) has prescriptive rules in the building code (ACI 318-19) meant to delay the onset of corrosion in aggressive environments; however, this same code considers structural capacity only in the pristine (non-corroded) state [5]. Due to climate change, coastal floods are predicted to become deeper and reach further inland, with damaging floods projected to occur 10 times as frequently as they do today within 30 years [6]. As a result, many structures that were not designed for aggressive environments may be subjected to them. Determining how the performance of structures in coastal environments evolves over time will be crucial in maintaining the safety of coastal communities.

This paper examines how an archetype RC moment frame's lateral strength and displacement capacity change over time due to different corrosion scenarios. Atmospheric corrosion and corrosion due to annual flooding are modeled. The results of the corrosion model are then used to inform the properties (remaining reinforcement area) of a structural model built using the open-source structural analysis software OpenSees [7]. Pushover analyses are performed on the moment frame in its new condition and after undergoing deterioration for 60 and 80 years due to atmospheric and flooding corrosion.

2 CORROSION MODELING

2.1 Corrosion stages

Corrosion of steel reinforcing bar embedded in concrete is modeled in two phases, initiation and propagation, as first proposed by Tuutti [8], with Li [9] further subdividing the propagation phase, as seen in Figure 1.

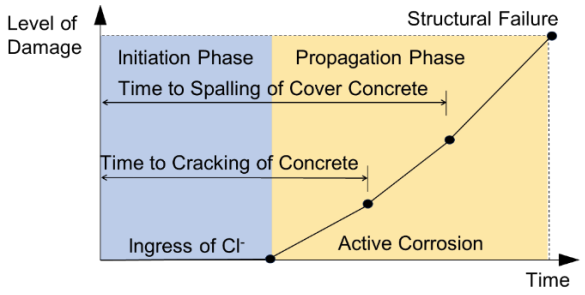

Figure 1: Corrosion phases in RC adapted from Li [9]

In pristine concrete, due to the high alkalinity of the pore solution, the steel reinforcement is protected by a passive oxide layer [8]. Localized corrosion begins once a critical concentration of chloride ions has reached the surface of the reinforcing steel, which breaks down the passive oxide layer. The initiation phase is characterized by the ingress of chloride ions through the cover concrete to the surface of the reinforcing steel, whereas the propagation phase is characterized by the active corrosion of the reinforcing steel.

2.2 Initiation phase

The transport of chlorides may occur through permeation, capillary absorption, and diffusion; however, diffusion is the most commonly observed mechanism. In this study, the initiation phase has been modeled as a purely diffusive process. In a diffusion-based model, chloride transport is caused by a concentration gradient in the concrete pore solution, which is governed by Fick's second law of diffusion [10]:

$$\frac{\partial C}{\partial t} = D\frac{\partial^2 C}{\partial x^2} \quad (1)$$

where, C is the concentration of chloride ions (either kg/m^3 or % weight of concrete), D (mm^2/s) is the diffusion coefficient of concrete, x (mm) is the distance from the nearest exposed concrete surface, and t (s) is the time during which diffusion occurs. Many researchers have

modeled the initiation phase using Crank's error function solution to Fick's second law of diffusion [11]:

$$C(x,t) = C_s\left[1 - \text{erf}\left(\frac{x}{2\sqrt{Dt}}\right)\right] \quad (2)$$

where, $C(x, t)$ is the chloride concentration at a distance x and time t, and C_s is the surface chloride concentration. The error function solution is based on the initial conditions of $C = C_s$ at $x \leq 0$, and $C = 0$ at $x > 0$. However, this solution does not allow for variation in the surface chloride concentration, making it suboptimal for capturing the effects of flooding.

Equation (1) may also be solved numerically using the Crank-Nicholson finite difference method [11], which allows for the surface chloride concentration to be updated at each timestep:

$$\begin{aligned} -rC_{i-1,t+1} + (2+2r)C_{i,t+1} \\ - rC_{i+1,t+1} \\ = rC_{i-1,t} \\ + (2-2r)C_{i,t} \\ + rC_{i+1,t} \end{aligned} \quad (3)$$

where, C_i is the chloride concentration at each distance interval i,

$$r = D\frac{dt}{(dx)^2} \quad (4)$$

dt is the time step, and dx is the distance step. The Crank-Nicholson method has been implemented to model the initiation phase in this study.

2.3 Rebar area loss

This study models rebar area loss in the propagation phase using the hemispherical pit model proposed by Val and Melchers [12]. In this model, the area of the corrosion pit is described by two intersecting circles, the rebar and another circle centered on the circumference of the rebar with a radius equal to the pitting depth $p(t)$, as seen in Figure 2.

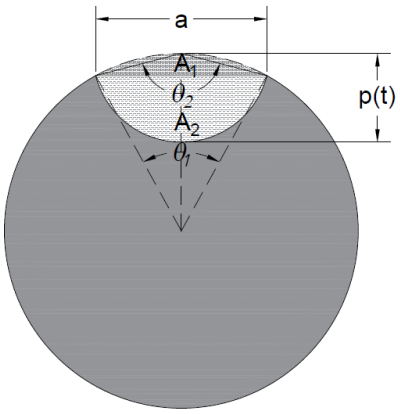

Figure 2: Hemispherical pit model adapted from Val and Melcher [12]

The area of the pit can be found using the geometry shown in Figure 2. $p(t)$ is given by the semi-empirical equation [12]

$$p(t) = \alpha * p(t)_{uniform} \quad (5)$$

where, α is an empirical pitting magnification factor. Gonzalez et al. [13] suggest a value between 4 and 8 for α as the pitting penetration is larger than uniform penetration for comparable mass loss. For this study, a value of 6 was used for α. The uniform penetration depth is calculated using Faraday's law of electrolysis [14]:

$$p(t)_{uniform} = \frac{M}{\rho n F}\int_{t_i}^{t} i_{corr}\,dt \quad (6)$$

where, M is the molar mass of iron (55.85 $g/mol\ Fe$), ρ is the density of iron (7.85 g/cm^3), n is the number of moles of electrons exchanged per mole of iron corroded (2 $mol\ e^-/mol\ Fe$), F is Faradays constant (96,485 $C/mol\ e^-$), t_i is the time at which corrosion initiates, t is the time at which the depth of corrosion is determined, and i_{corr} is the corrosion current density. Substituting equation (6) into equation (5), for $p(t)$ in mm, with t in years and i_{corr} in $\mu A/cm^2$, leads to

$$p(t) = 0.0116\alpha\int_{t_i}^{t} i_{corr}\,dt \quad (7)$$

2.4 Corrosion current density

Equation (7) shows that i_{corr} is a key parameter for determining the pitting depth

and rebar mass loss. Many models of varying complexity have been proposed in the literature to determine i_{corr}. A relatively simple model has been adopted here. During the initiation phase, the corrosion current density is assumed to be zero regardless of the chloride exposure (atmospheric or annual flooding). During the propagation stage, for RC structural elements exposed to only atmospheric chlorides, an average corrosion current density of 0.75 $\mu A/cm^2$ is assumed before the cover concrete cracking, as suggested by Andrade [15]. After cover cracking, due to easier access for oxygen and water to the rebar, the corrosion current density is assumed to increase until it has doubled and until a critical crack width has been reached [16].

For RC structural elements subjected to annual flooding, the average corrosion current density before cracking is assumed to be 1 $\mu A/cm^2$ during the corrosion propagation phase. This higher rate is assumed to account for slightly greater saturation of the concrete pores due to flooding, resulting in lower resistivity than the non-flooded concrete. After cracking, two scenarios are considered, a lower-bound (LB) where the rate doubles like the non-flooded concrete, and an upper-bound (UB), where, due to the corrosion products being washed out of the cracks by the flooding, the rate increases to four times the pre-crack rate, and reaches rates similar to those for open-air corrosion [17]. These assumptions can be refined as data on corrosion due to flooding becomes available, which is currently unavailable to the authors' best knowledge.

2.5 Concrete cracking

Concrete cracking is simulated by modeling the rebar and the surrounding concrete as a thick-walled cylinder with a porous zone surrounding the rebar to account for corrosion products dispersing into the concrete pores before beginning to exert pressure. The pressure due to corrosion products is calculated as suggested by El Maaddawy and Soudki [18]:

$$P_{cor} = \frac{r_l E_{ef} d_r}{90.9\left(\frac{r_i^2 + r_e^2}{r_e^2 - r_i^2} + \upsilon\right)(d_r + 2\delta_0)} - \frac{2\delta_0 E_{ef}}{\left(\frac{r_i^2 + r_e^2}{r_e^2 - r_i^2} + \upsilon\right)(d_r + 2\delta_0)} \quad (8)$$

where, P_{cor} is the pressure due to corrosion products in MPa, r_l is the percentage of rebar mass or area loss, δ_0 is the thickness of the porous zone in mm, d_r is the uncorroded diameter of the rebar in mm, r_i is the uncorroded radius of the rebar plus δ_0 in mm, r_e is the cover thickness plus the uncorroded radius of the rebar in mm, υ is Poison's ratio for concrete, and E_{ef} is the effective modulus of elasticity for concrete in MPa.

The crack width growth due to corrosion is modeled based on the area loss of longitudinal rebar. The correlation between crack width and rebar loss was found by Vidal et al. [19] to be:

$$w = 0.575(\Delta A_r - \Delta A_{r0}) \quad (9)$$

where, w is the crack width in mm, ΔA_r is the rebar cross-sectional area loss in mm^2, and ΔA_{r0} is the rebar cross-sectional area loss at crack initiation in mm^2.

The corrosion model properties that are independent of the structure are summarized in Table 1 for three corrosion cases: atmospheric (Atm), lower-bound annual flooding (Flood LB), and upper-bound annual flooding (Flood UB).

Table 1: Corrosion model inputs

Scenario	Atm	Flood LB	Flood UB
Surface Cl^- (% weight)	0.6 [20]	0.8	0.8
Pre-cracking i_{corr} ($\mu A/cm^2$)	0.75 [15]	1	1
Post-/Pre-cracking i_{corr} ratio	2 [16]	2 [16]	4 [21]

3 RC STRUCTURE ARCHETYPE

The structure archetype used in this study is a two-dimensional RC moment frame designed according to ASCE 7-02 by Hasselton [22]. The moment frame is an interior frame rather than a perimeter frame, meaning only the end columns are exterior columns. Table 2 shows the key geometric and design properties of the moment frame.

Table 2: RC Moment frame properties

Number of stories	4
Number of bays	3
Story height (m)	4.6 (1st story), 4 (2nd to 4th stories)
Bay width (m)	9.1
Concrete compressive strength (MPa)	35
Rebar yield strength (MPa)	420
Column/beam longitudinal rebar diameter (mm)	28.7
Exterior column reinforcement ratio	0.013 (1st & 2nd story) 0.011 (3rd & 4th story)
Interior column reinforcement ratio	0.016 (1st to 3rd story) 0.011 (4th story)
Column/beam transverse rebar diameter (mm)	12.7
Column/beam clear cover (mm)	38
Column dimensions (mm)	762x762
Beam dimensions (mm)	762×762 (2nd and 3rd stories), 610×762 (4th story and roof)

4 CORROSION MODEL RESULTS

The corrosion model is run for atmospheric, Flood LB, and Flood UB corrosion cases on the columns of the archetype. Figure 3 shows the corrosion current density as a function of time and identifies the times corresponding to corrosion initiation, cover cracking, and attainment of critical crack width.

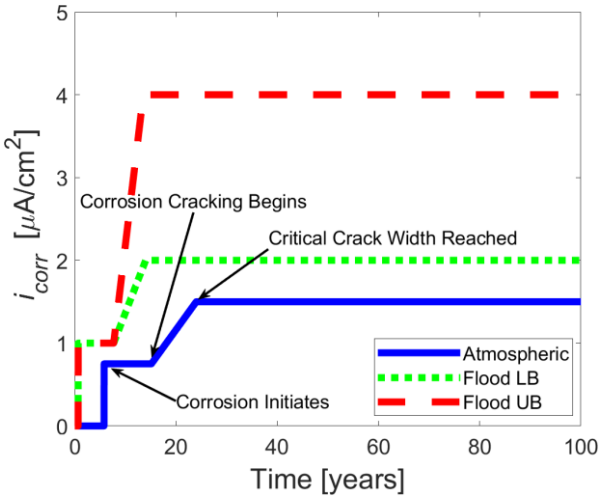

Figure 3: Changes in corrosion current over time

As seen in Figure 3, not only do columns subjected to annual flooding have a higher initial corrosion rate (1 $\mu A/cm^2$ as opposed to 0.75 $\mu A/cm^2$), but the columns undergoing purely atmospheric corrosion also take longer to initiate than either of the annual flooding cases.

Figure 4 shows the percentage of rebar area remaining for both the transverse and longitudinal rebar. At the locations of most extreme pitting, the transverse rebar is seen to be corroded entirely in the Flood UB scenario by 60 years. In contrast, 45% of the transverse rebar area remains in the Flood LB scenario, and 75% remains in the atmospheric corrosion scenario. A similar, though less extreme, trend for the longitudinal rebar is seen, with 60% rebar area remaining for Flood UB, 87% for Flood LB, and 94% for the atmospheric corrosion scenario after 60 years.

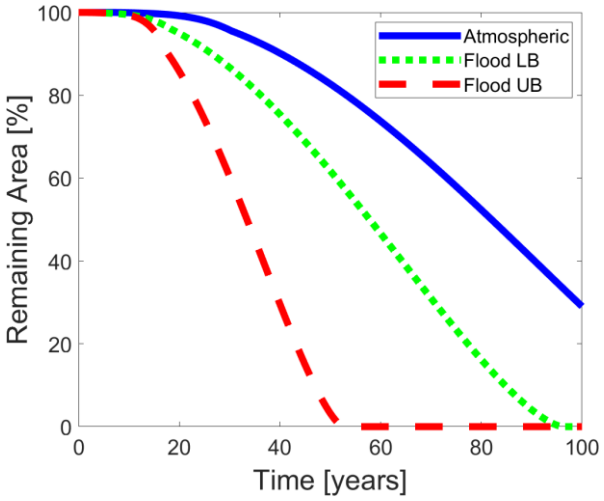

a) Transverse rebar

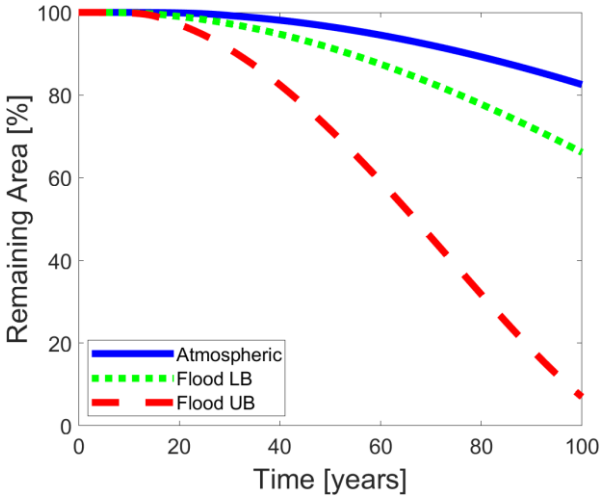

b) Longitudinal rebar

Figure 4: Remaining rebar percentages

5 STRUCTURE MODEL

The archetype is modeled in OpenSees [7], using linear-elastic beam-column elements for the beams and columns with all non-linearity lumped in plastic hinges at the ends of beams and columns. The plastic hinges are modeled using the Ibarra-Medina-Krawinkler deterioration model [23]. The gravity load is applied to a leaning column to model P-Delta effects. Figure 5 shows the frame as it is modeled in OpenSees.

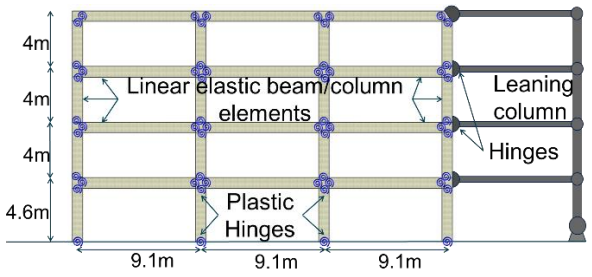

Figure 5: Structural model of the moment frame

The structural response of the archetype is significantly affected by the behaviors of the plastic hinges as defined by their moment and rotational capacities, which are determined using empirical equations [22]. Reduced rebar cross-sectional areas are used for corroded columns in these equations. Although the reduced rebar area decreases the moment capacity at yielding and the rotation capacity at peak moment, the ratio of the moment capacity to yield moment (M_{cap}/M_y) is not affected by the rebar area in these equations. This results in a higher post-yield stiffness in corroded columns than in the pristine columns, which is physically unlikely. Therefore, the post-yield stiffness of the corroded elements is adjusted to be the same as that of the non-corroded elements. Figure 6 shows an example of the plastic hinge inputs for first-floor columns in the pristine state at 0 years and after 80 years of atmospheric and flooding corrosion. The interior columns of the frame have larger axial loads than the exterior columns, resulting in a larger reinforcement ratio and moment capacity. Additionally, atmospheric corrosion is assumed to affect only the exterior columns.

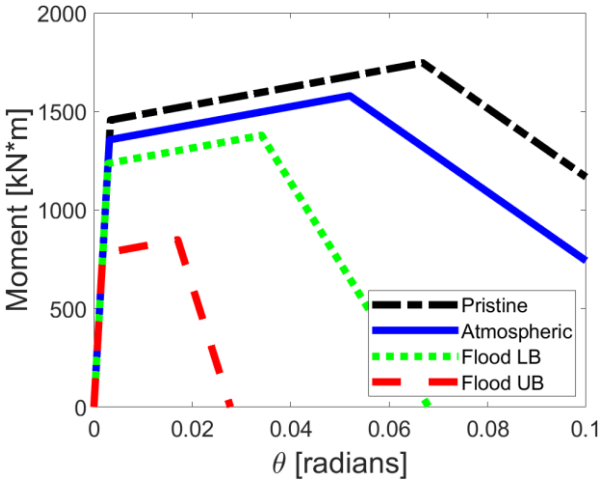

a) Exterior columns

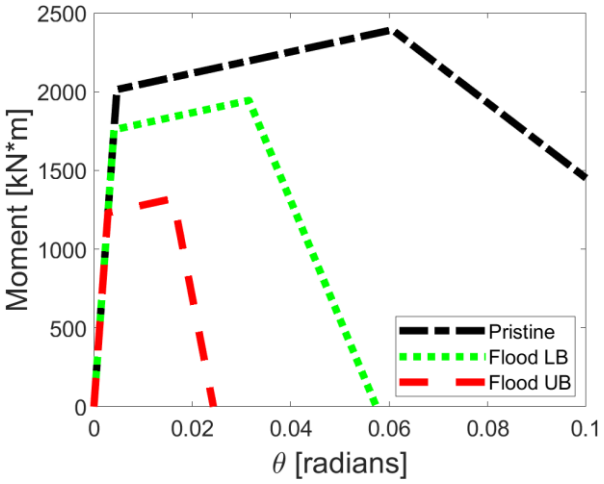

b) Interior columns

Figure 6: First floor column hinges at 80 years

6 ANALYSIS CASES

The archetype frame is analyzed in its pristine state at 0 years and after 60 and 80 years of exposure, as described in Table 3. In all the cases except for the pristine condition, the exterior columns on the 2nd-4th floors are subjected to atmospheric corrosion only. The interior columns and all the beams are assumed to be unaffected by atmospheric corrosion.

Table 3: Corrosion cases analyzed

Corrosion Case	1st Floor Exterior Columns	1st Floor Interior Columns
Atm	Atmospheric	No Corrosion
LB Ext	Flood LB	No Corrosion
LB All	Flood LB	Flood LB
UB Ext	Flood UB	No Corrosion
UB All	Flood UB	Flood UB

7 RESULTS

Figure 7 shows the base shear-roof drift ratio (ratio of roof lateral displacement to roof height) of the pristine frame at 0 years and the frame after 60 and 80 years of atmospheric corrosion. The lateral strength and displacement capacity decrease insignificantly (less than 1%) due to atmospheric corrosion compared to the pristine state even after 80 years. Displacement capacity (Δ_{cap}) is defined as the displacement at the lateral strength (maximum base shear) throughout the paper.

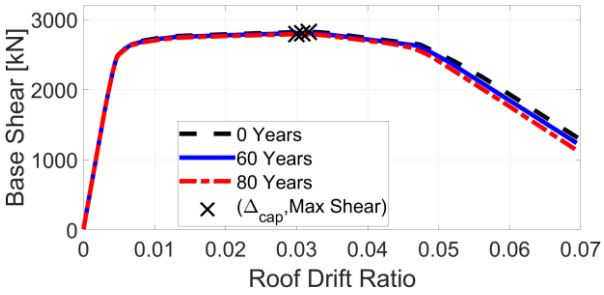

Figure 7: Pushover analyses results of the frame under atmospheric corrosion

Figure 8 shows the base shear-roof drift relationship of the frame when exposed to atmospheric corrosion on the upper floors and lower-bound flooding corrosion of the columns on the 1st floor. Figure 8a shows that after 80 years, there is a 2% reduction in lateral strength and an 11% reduction in displacement capacity when only exterior columns flood under the lower-bound flooding scenario. Figure 8b indicates that when all columns

flood, instead of just the exterior columns, lower-bound flooding corrosion leads to a 4% reduction in peak lateral strength and a 21% reduction in displacement capacity after 80 years.

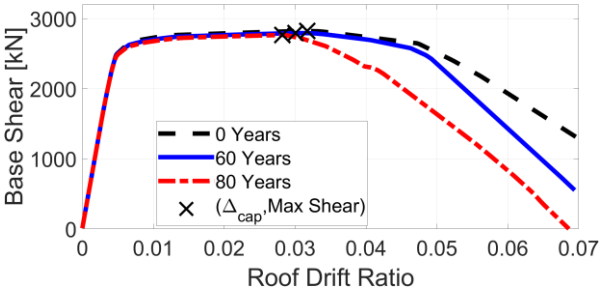

a) Only exterior columns flood

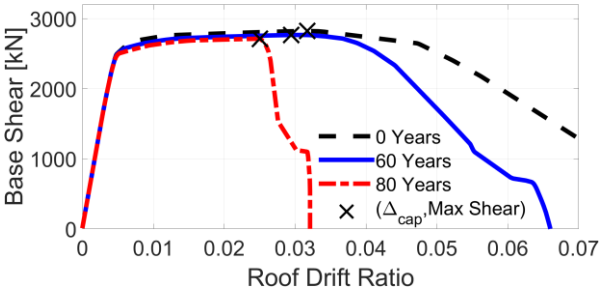

b) All columns flood

Figure 8: Pushover analyses results under atmospheric and lower-bound flooding-related corrosion

Figure 9 shows the pushover analyses results for the RC frame exposed to atmospheric corrosion and upper-bound flooding corrosion for 60 and 80 years compared to the pristine frame at 0 years. When only the first-floor exterior columns flood (Figure 9a), the frame experiences a 4% and 8% loss of lateral strength after 60 and 80 years, respectively, compared to its pristine state. The displacement capacity drops 52% after 60 years and 64% after 80 of corrosion. When all first-floor columns flood (Figure 9b), the most dramatic reductions are observed with lateral strength reducing 9% and 26% after 60 and 80 years, respectively. In this case, the displacement capacity reduces by 60% at 60 years and 83% at 80 years.

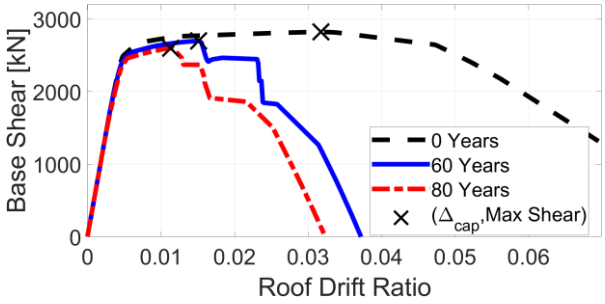

a) Only exterior columns flood

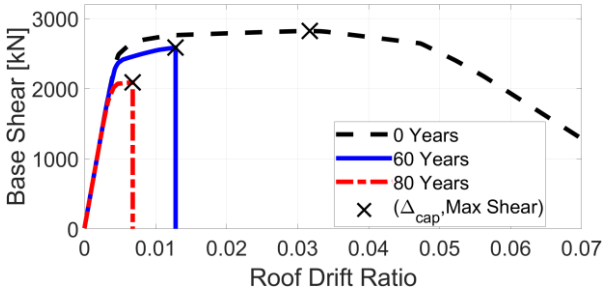

b) All columns flood

Figure 9: Pushover analyses results under atmospheric and upper-bound flooding-related corrosion

The two parameters that have the greatest impact on the lateral performance of the moment frame are the number of columns affected (only the exterior columns versus all the columns) and the post-cracking corrosion rate. The lower-bound flooding corrosion scenarios show that the decrease in displacement capacity after 80 years doubles when all first-floor columns corrode instead of only the exterior columns corroding. The post-cracking corrosion rate has an even larger effect on the lateral performance of the structure, with a decrease in displacement capacity after 80 years for the upper-bound flooding corrosion that is 6 times that of lower-bound flooding corrosion when only the exterior columns are corroded and 4 times greater when all columns are corroded.

The displacement capacity decreases more than lateral strength due to reinforcement corrosion. This is likely due to the large loss of transverse rebar area observed in Figure 4a. With the transverse rebar corroded significantly, it no longer provides effective confinement for the core, decreasing the displacement capacity.

8 CONCLUSIONS

Corrosion is modeled for the columns of an archetype RC moment frame considering both atmospheric corrosion of exterior columns throughout the frame height and annual coastal flooding of the first-floor exterior columns or all columns. An average pre-crack corrosion current density with lower and upper-bound post-cracking corrosion current densities is assumed to model the corrosion due to flooding. The main conclusions are:

- Atmospheric corrosion takes longer to initiate than corrosion due to annual flooding.
- Lateral strength reduction is much greater due to flooding-related corrosion (26% in the worst-case scenario considering the upper-bound flooding corrosion and flooding of all columns) compared to atmospheric corrosion (1%) after 80 years.
- Displacement capacity is even more affected by flooding than lateral strength (83% reduction in the worst-case scenario considering the upper-bound flooding corrosion and flooding of all columns), but it remains virtually unchanged (<1%) due to atmospheric corrosion after 80 years.
- Displacement capacity loss is primarily attributed to the loss of transverse rebar area.

ACKNOWLEDGEMENTS

This material is based upon work supported by the National Science Foundation, Award No. CMMI 2245401. All opinions expressed are the authors' and do not necessarily reflect the policies and views of the sponsors.

REFERENCES

[1] Wright, D.G., R. Pawlowicz, T.J. McDougall, R. Feistel, and G.M. Marion, 2011. Absolute Salinity, "Density Salinity" and the Reference-Composition Salinity Scale: present and future use in the seawater standard TEOS-10. *Ocean science*, **7**(1): p. 1-26.

[2] Murphy, D.M., K.D. Froyd, H. Bian, C.A. Brock, J.E. Dibb, J.P. DiGangi, G. Diskin, M. Dollner, A. Kupc, E.M. Scheuer, G.P. Schill, B. Weinzierl, C.J. Williamson, and P. Yu, 2019. The distribution of sea-salt aerosol in the global troposphere. *Atmospheric chemistry and physics*, **19**(6): p. 4093-4104.

[3] *National Risk Index/Coastal Flooding*. [cited 2024; Available from: https://hazards.fema.gov/nri/coastal-flooding.

[4] 2018 *Long-Term National Seismic Hazard Map*. [cited 2024; Available from: https://www.usgs.gov/media/images/2018-long-term-national-seismic-hazard-map.

[5] 2019. *Building code requirements for structural concrete (ACI 318-19) : commentary on building code requirements for structural concrete (ACI 318R-19)*. Building code and commentary. Farmington Hills, Mich: American Concrete Institute.

[6] Sweet, W., 2022. *Global and regional sea level rise scenarios for the United States : updated mean projections and extreme water level probabilities along U.S. coastlines*. Updated mean projections and extreme water level probabilities along U.S. coastlines. Silver Spring, Maryland: National Oceanic and Atmospheric Administration, U.S. Department of Commerce, National Ocean Service.

[7] McKenna, F., Fenves, G. L, and Scott, M. H. , 2000, *Open system for earthquake engineering simulation*.

University of California, Berkeley: University of California, Berkeley.

[8] Tuutti, K., 1982, *Corrosion of Steel in Concrete*, in *Division of Building Materials*: Swedish Cement and Concrete Research Institute, Stockholm. p. 468.

[9] Qing Li, C., 2004. Reliability Based Service Life Prediction of Corrosion Affected Concrete Structures. *Journal of structural engineering (New York, N.Y.)*, **130**(10): p. 1570-1577.

[10] Fick, A., 1855. V. On liquid diffusion. *The London, Edinburgh, and Dublin Philosophical Magazine and Journal of Science*, **10**(63): p. 30-39.

[11] Crank, J., 1979. *The mathematics of diffusion*. 2d ed. Oxford science publications. Oxford [Eng: Clarendon Press.

[12] Val, D.V. and R.E. Melchers, 1997. Reliability of Deteriorating RC Slab Bridges. *Journal of structural engineering (New York, N.Y.)*, **123**(12): p. 1638-1644.

[13] González, J.A., C. Andrade, C. Alonso, and S. Feliu, 1995. Comparison of rates of general corrosion and maximum pitting penetration on concrete embedded steel reinforcement. *Cement and Concrete Research*, **25**(2): p. 257-264.

[14] Cao, C., M.M.S. Cheung, and B.Y.B. Chan, 2013. Modelling of interaction between corrosion-induced concrete cover crack and steel corrosion rate. *Corrosion science*, **69**: p. 97-109.

[15] Andrade, C., 2023. Steel corrosion rates in concrete in contact to sea water. *Cement and Concrete Research*, **165**: p. 107085.

[16] Wang, H., R. Ranade, and P. Okumus, 2023. Calibrating a Physics-Based Corrosion Model with Field-Based Bridge Condition Data. *Journal of bridge engineering*, **28**(5).

[17] Morcillo, M. 1995. *Atmospheric Corrosion in Ibero-America: The MICAT Project*. in W.W. Kirk and H.H. Lawson, Editors. *Atmospheric Corrosion, ASTM STP 1239*. Philadelphia, PA American Society for Testing and Materials, International. p. 257-275.

[18] El Maaddawy, T. and K. Soudki, 2007. A model for prediction of time from corrosion initiation to corrosion cracking. *Cement & concrete composites*, **29**(3): p. 168-175.

[19] Vidal, T., A. Castel, and R. François, 2004. Analyzing crack width to predict corrosion in reinforced concrete. *Cement and concrete research*, **34**(1): p. 165-174.

[20] Life-365^{TM}, 2020, *Life-365 service life prediction model^{TM}*. Life-365 Consortium.

[21] Morcillo, M., W.W. Kirk, and H.H. Lawson. 1995. *Atmospheric Corrosion in Ibero-America: The MICAT Project*. 100 Barr Harbor Drive, PO Box C700, West Conshohocken, PA 19428-2959: ASTM International. p. 257-275.

[22] Haselton, C.B., G.G. Deierlein, and C. Pacific Earthquake Engineering Research, 2008, *Assessing seismic collapse safety of modern reinforced concrete moment-frame buildings*. Pacific Earthquake Engineering Research Center: Berkeley, Calif.

[23] Ibarra, L.F., R.A. Medina, and H. Krawinkler, 2005. Hysteretic models that incorporate strength and stiffness deterioration. *Earthquake engineering & structural dynamics*, **34**(12): p. 1489-1511.